Influence of α-clustering configurations in $^{16}O + ^{197}Au$ collisions at Fermi energy

Chen-Chen Guo (郭琛琛),[1,2] Yu-Gang Ma (马余刚),[3,1,*] Zhen-Dong An (安振东),[1,4] and Bo-Song Huang (黄勃松)[1]

[1]*Shanghai Institute of Applied Physics, Chinese Academy of Sciences, Shanghai 201800, China*

[2]*Sino-French Institute of Nuclear Engineering and Technology, Sun Yat-sen University, Zhuhai 519082, China*

[3]*Key Laboratory of Nuclear Physics and Ion-beam Application (MOE), Institute of Modern Physics, Fudan University, Shanghai 200433, China*

[4]*School of Physics and Astronomy, Sun Yat-sen University, Zhuhai 519082, China*

(Received 18 August 2018; revised manuscript received 19 February 2019; published 18 April 2019)

The α-clustering configurations in light nuclei have attracted a great deal of attention over past years. Nuclear reactions serve as one possible way to study this topic. The aim of this paper was to discuss whether or not heavy-ion collisions at Fermi energy could be a good tool to investigate the cluster configurations in light nuclei. In particular, $^{16}O + ^{197}Au$ collisions are simulated using a transport model to check if any observable change is sensitive to the cluster configurations. Within an extended quantum molecular dynamics model, two different α-clustering configurations (chain and tetrahedron) of ^{16}O were employed in the initialization. $^{16}O + ^{197}Au$ collisions at a beam energy of 40 MeV/nucleon with an impact parameter of 3 fm were simulated; then the collective flow parameters (v_1, v_2, v_3, and v_4) of free protons were analyzed as a function of both the rapidity and the transverse momentum. It was found that flow parameters (v_1, v_2, v_3, and v_4) decrease with an increase of the flow order, and that the difference in the flow parameters of free protons caused by the initial α-clustering configurations increases with transverse momentum. In the higher transverse momentum region (0.2–0.25 GeV/c), these flow patterns are quite sensitive to the initial α-clustering configurations, and can be regarded as sufficiently sensitive probes that can be used to study the clustering configurations in light nuclei.

DOI: 10.1103/PhysRevC.99.044607

I. INTRODUCTION

In recent years, more *ab initio* methods have been developed and applied to investigate the properties of nuclei, and some novel structures of nuclei have been predicted. The rapid development of rare isotope facilities all over the world (such as the FRIB in the United States, the SPIRAL2 in France, the TRIUMF in Canada, the RIBF at RIKEN in Japan, ROAN in South Korea [1], and HIAF in China [2]) has made possible the experimental study of novel nuclear structures. The α-clustering phenomenon in some specific nuclei is one of the novel structures that has attracted substantial attention in recent years [3,4]. In fact, the idea that some nuclei might be composed of α particles was suggested long ago [5], but not much attention was paid until the 1960s, due to the failure of the single-particle shell model when describing the properties of excited states of some nuclei with equal numbers of neutrons and protons (e.g., ^{12}C and ^{16}O) [6]. Since then, much progress has been made in this field [7–18]. Even though extensive studies have been carried out to extract information about α clusters in light nuclei, a deeper understanding of the clustering structure of nuclei, from both experimental and theoretical perspectives, is still one of the greatest challenges in nuclear science [19].

Nuclear reactions serve as one important way to study the α-clustering structure. For example, with an extended quantum molecular dynamics (EQMD) model [20], which is also a microscopic dynamical model, the α-clustering effect on the giant dipole resonance [17,21], photonuclear reaction in quasideuteron regime [22,23], and collective flows in $^{16}O + ^{16}O$ at Fermi energy [24] have been investigated. Different α-clustering configurations at the initial stage have been found to affect the reaction after which differences in the final observables (such as momentum spectra, directed and elliptic flows) with different α-clustering configurations can be observed. Moreover, at relativistic energies, $^{12}C + Au$ collisions were investigated using a multiphase transport model with the different α-clustering configurations of ^{12}C [25–27]. It was found that the elliptic and triangular flows are sensitive to the initial α-clustering configurations.

In this work, within the EQMD model, the influence of the α-clustering configurations on the collective flow produced in an asymmetric nuclear reaction, such as $^{16}O + ^{197}Au$ at the selected Fermi energy, was investigated. The paper is arranged as follows: in Sec. II, features of the EQMD transport model are described. Results and discussion for the effect of the α-clustering configurations on collective flows are then presented in Sec. III. Finally, the article is summarized in Sec. IV.

II. MODEL DESCRIPTION

The quantum molecular dynamics (QMD) model [28,29] is a microscopic dynamical n-body model that has been successful in describing nuclear reactions at intermediate energies. Various extensions based on a QMD model have been

*Corresponding author: mayugang@cashq.ac.cn

made afterwards for further improvement, e.g., the improved quantum molecular dynamics (ImQMD) model [30] and the Lanzhou quantum molecular dynamics (LQMD) model [31]. The EQMD model is based on the same principles as QMD, but in order to better study nuclear reactions at low energy around the Coulomb barrier, several improvements were made by Maruyama *et al.*, in which work the details can be found [20]. Among those improvements, the most important ones include a phenomenological Pauli potential in effective nucleon-nucleon interactions, as well as the dynamical width of each nucleon wave packet. With those improvements, the model can well describe ground-state properties such as binding energies and the density profiles or α-clustering structure in light nuclei [20].

Each nucleon in the EQMD model is represented by a Gaussian wave packet in phase space as follows:

$$\phi_i(\mathbf{r};t)=\left(\frac{\nu_i+\nu_i^*}{2\pi}\right)^{3/4}\exp\left[-\frac{\nu_i}{2}[\mathbf{r}-\mathbf{r}_i(t)]^2+\frac{i}{\hbar}\mathbf{r}\cdot\mathbf{p}_i(t)\right], \tag{1}$$

where $\mathbf{r}_i(t)$ and $\mathbf{p}_i(t)$ are the centers of a wave packet of nucleons i in the coordinate and momentum space, respectively. Moreover, the total wave function of the system, which is a direct product of the Gaussian wave packets of nucleons, is written as

$$\Psi=\prod_i \phi_i(\mathbf{r}_i). \tag{2}$$

In the traditional QMD model, the width of the Gaussian wave packet is fixed and time independent, while in the EQMD model, the width of the Gaussian wave packet is a complex with the form

$$\nu_i \equiv \frac{1}{\lambda_i}+i\delta_i, \tag{3}$$

where λ_i and δ_i are its real and imaginary parts, respectively, which are also time dependent.

The Hamiltonian of the system H consists of the kinetic energy T and the effective interaction potential energy $H_{\rm int}$,

$$H=T+H_{\rm int}, \tag{4}$$

where $H_{\rm int}$ contains several parts as follows:

$$H_{\rm int}=H_{\rm Skyrme}+H_{\rm Coulomb}+H_{\rm Symmetry}+H_{\rm Pauli}. \tag{5}$$

The Pauli potential $H_{\rm Pauli}$ is used to compensate partly the missed antisymmetrization in the total wave function and it has the form

$$H_{\rm Pauli}=\frac{c_P}{2}\sum_i (f_i-f_0)^\mu\theta(f_i-f_0), \tag{6}$$

$$f_i\equiv\sum_j \delta(S_i,S_j)\delta(T_i,T_j)|\langle\phi_i|\phi_j\rangle|^2, \tag{7}$$

where f_i denotes the overlap of the wave packets of nucleons i with the same spin and isospin. The equations of motion of the EQMD are determined by the time-dependent variational principle,

$$\begin{aligned}
\dot{\mathbf{R}}_i &= \frac{\partial H}{\partial \mathbf{P}_i}+\mu_{\mathbf{R}}\frac{\partial H}{\partial \mathbf{R}_i},\\
\dot{\mathbf{P}}_i &= -\frac{\partial H}{\partial \mathbf{R}_i}+\mu_{\mathbf{P}}\frac{\partial H}{\partial \mathbf{P}_i},\\
\frac{3\hbar}{4}\dot{\lambda}_i &= -\frac{\partial H}{\partial \delta_i}+\mu_\lambda\frac{\partial H}{\partial \lambda_i},\\
\frac{3\hbar}{4}\dot{\delta}_i &= \frac{\partial H}{\partial \lambda_i}+\mu_\delta\frac{\partial H}{\partial \delta_i}.
\end{aligned} \tag{8}$$

Here $\mu_{\mathbf{R}}$, $\mu_{\mathbf{P}}$, μ_λ, μ_δ are damping coefficients. With negative values of these coefficients, the system goes to its local minimum point. In the beginning, the phase space of nucleons is obtained initially from a random configuration. After that, a frictional cooling method is used to get the energy-minimum state. The initialized projectile and target are quite stable and no nucleons will escape before they touch each other. The model can describe the ground-state properties, such as binding energy and rms radius, quite well over a very wide mass range [32,33]. One can get different initial states for α-conjugated light nuclei (energy-minimum state); then one can select different initial configurations (such as chain, tetrahedral, square, or kite for ^{16}O) by hand for further study [17,21].

III. RESULTS AND DISCUSSION

First of all, to show the capability of the EQMD model to describe the existing data, we display in Fig. 1 the charge multiplicity distributions in collisions of ^{12}C + ^{197}Au (a),

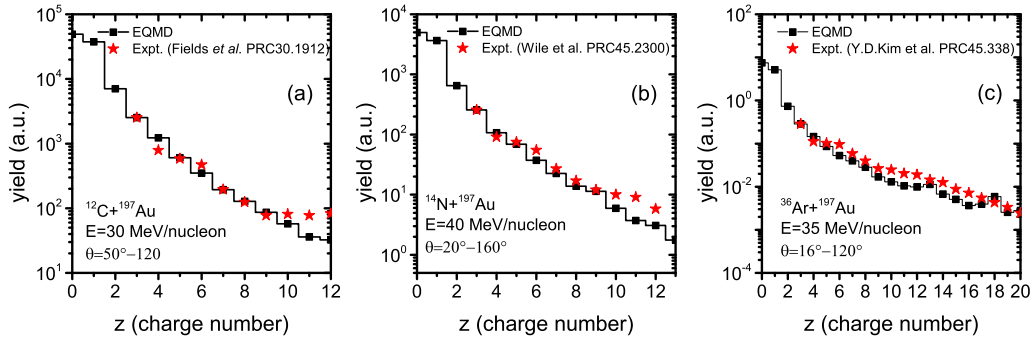

FIG. 1. Charge multiplicity distributions in collisions of ^{12}C + ^{197}Au (a), ^{14}N + ^{197}Au (b), and ^{36}Ar + ^{197}Au (c) around the Fermi energy. The experimental data from Refs. [34–36] are shown by stars, calculations with the EQMD model under the same reaction conditions as for these experimental data are shown by solid lines.

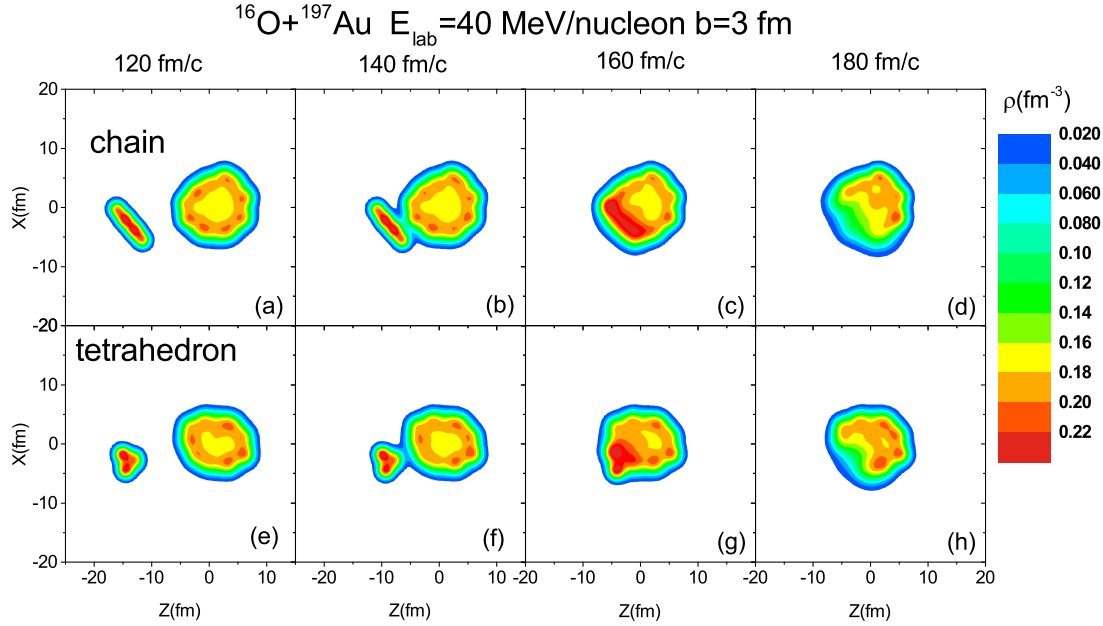

FIG. 2. Contour plots of the nucleon density in the x-z reaction plane produced from $^{16}\mathrm{O}+{}^{197}\mathrm{Au}$ collisions at 40 MeV/nucleon with impact parameters $b = 3$ fm. Simulations with the chain [upper panels, (a)–(d)] and tetrahedron [lower panels, (e)–(h)] configurations at four different evolution times (120, 140, 160, and 180 fm/c) are shown. Here only one random event is displayed.

$^{14}\mathrm{N}+{}^{197}\mathrm{Au}$ (b), and $^{36}\mathrm{Ar}+{}^{197}\mathrm{Au}$ (c) around the Fermi energy [34–36]. In these calculations, a simple coalescence method is used to recognize clusters. A proton-proton pair with relative distance (ΔR_{pp}) smaller than 2.8 fm, or a neutron-neutron (proton) pair (ΔR_{np}) with relative distance smaller than 3.8 fm, and relative momentum (ΔP) smaller than 0.25 GeV/c, are considered to belong to the same fragment. It is noteworthy that the changes in the above coalescence parameters in a suitable range (e.g., taking $\Delta R_{pp} = \Delta R_{np} = 1.5$ to 2.5 fm, and $\Delta P = 0.2$–0.25 GeV/c) have little effect on the flow results. It can be seen that, with normalization at $Z = 3$, the overall dependence on Z can be well reproduced. We note that the charge multiplicity distribution could be influenced by the Pauli potential and the chosen parameters in the coalescence algorithm, as discussed in Refs. [37,38]. Therefore, it is not used as an observable indicator for probing the α-clustering configurations. Concerning the effect on flow, we have determined that the influence of the previously mentioned coalescence parameters is quite weak. A very similar result was obtained in Refs. [39] where the effect of the coalescence parameters on the flow has been studied. The inclusion of the Pauli potential prevents nucleons with the same spin and isospin from coming close in the phase space. Because only the flow of free protons (i.e., protons which are far from each other in phase space) was investigated in this work, its influence on the flow of free protons is less important. In Ref. [40], within a QMD model, the authors also demonstrate that the magnitude of the collective flow is only slightly affected by the Pauli potential.

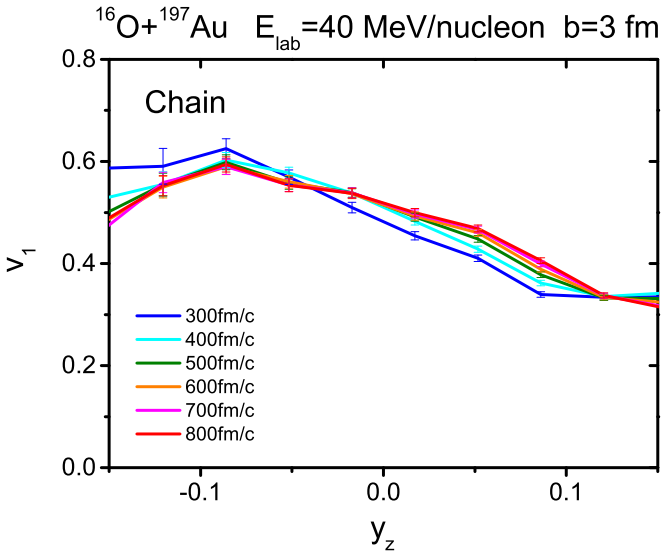

FIG. 3. The directed flow of free protons produced in a $^{16}\mathrm{O}+{}^{197}\mathrm{Au}$ collision at 40 MeV/nucleon and $b = 3$ fm. The results at different times are shown by different lines.

To obtain the general information of collisions with different initial α-clustering configurations, we tested the evolution of nucleon density during the dynamic process. Figure 2 shows the time evolution of the density contour plots for $^{16}\mathrm{O}+{}^{197}\mathrm{Au}$ collisions at 40 MeV/nucleon with impact parameter $b = 3$ fm. Calculations were performed using the chain (upper panels) and tetrahedron (lower panels) α-clustering configurations. The initial distance between the centers of the projectile and target nuclei was set to 50 fm; thus the target and projectile touch each other at about 140 fm/c. It can be seen from the chain and tetrahedron configurations of projectiles from initialization that these configurations can be quite stable before collision with a projectile. It should be noted that, to see different α-clustering configurations in the initialization, only a single random event was used for

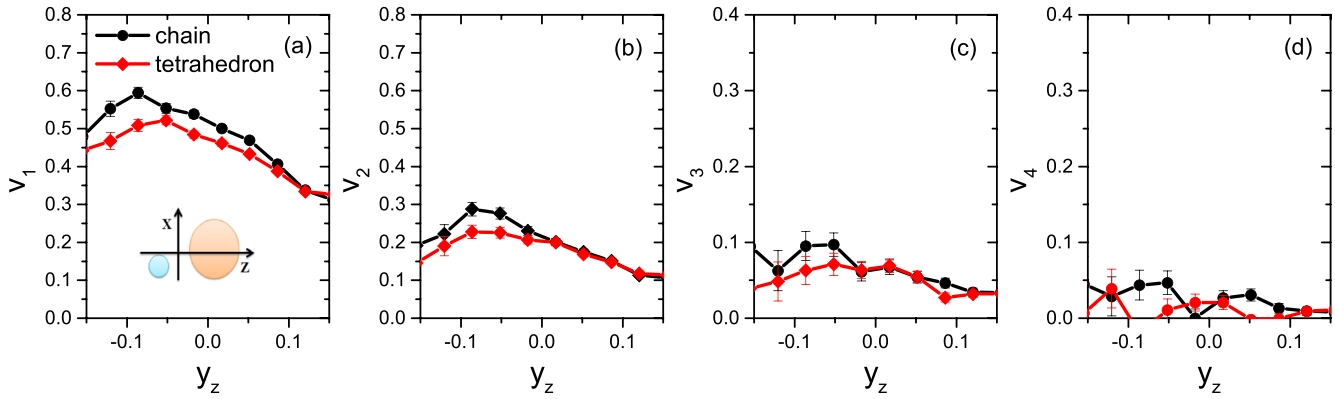

FIG. 4. The flow parameters v_1, v_2, v_3, and v_4 of free protons as a function of rapidity y_z for $^{16}O + ^{197}Au$ collisions at 40 MeV/nucleon and $b = 3$ fm. The calculations obtained with the chain and tetrahedron configurations of ^{16}O are shown by solid circles and solid diamonds, respectively.

drawing Fig. 2. However, to study its influence on final observables, 30 000 events for each configuration were simulated, and a random rotation angle of the initialized α-clustering configurations was used for each event.

From Fig. 2 we can see that the projectile and target touch each other before 200 fm/c. Now we check the time evolution of the flow. As an example, we take the directed flow parameter $v_1 = \langle \cos(\phi) \rangle = \langle \frac{p_x}{p_t} \rangle$, where $p_t = \sqrt{p_x^2 + p_y^2}$ is the transverse momentum of emitted particles, and p_x is the x component of momentum, as a function of rapidity ($y_z = \frac{1}{2} \ln \frac{E+p_z}{E-p_z}$) at different reaction time which is shown in Fig. 3. One can see that the flow is basically stable after 400 fm/c; therefore, we think that 800 fm/c is long enough to extract collective flows. Then Fig. 4 shows the collective flow parameters v_1, $v_2 = \langle \cos(2\phi) \rangle = \langle (\frac{p_x}{p_t})^2 - (\frac{p_y}{p_t})^2 \rangle$, $v_3 = \langle \cos(3\phi) \rangle = \langle \frac{4{p_x}^3 - 3p_x{p_t}^2}{{p_t}^3} \rangle$, and $v_4 = \langle \cos(4\phi) \rangle = \langle \frac{{p_t}^4 - 8{p_x}^2{p_t}^2 + 8{p_x}^4}{{p_t}^4} \rangle$ of free protons as a function of the rapidity. Here p_y is the y component of momentum, p_z is the z component of momentum, and E is the total energy in the center-of-mass system. Usually, the x axis is defined to be along the impact parameter vector and the y axis is perpendicular to that in the reaction plane, with the z axis along the beam direction. The cutoff time of the calculated results we chose here was 800 fm/c as we explained above, which is long enough for reaction evolution. Therefore, it was not necessary to use a deexcitation process, e.g., followed by an afterburner process [41]. It should be noted that, for mass symmetric collision, the v_1 and v_3 flows are odd functions of the center-of-mass rapidity, and the v_2 and v_4 are even functions of the center-of-mass rapidity. However, for a mass asymmetric nuclear reaction, they are neither odd nor even, as can be observed in Fig. 4. It was found that the flow parameters (v_1, v_2, v_3, and v_4) calculated with the chain configuration are slightly larger than those with the tetrahedron configuration, but the difference between them steadily decreases with increasing order of flows. Because a random rotation angle of the initialized α-clustering configurations is taken for each event, the impact of the initial configurations on the final observable is largely washed out. Moreover, the impact parameter used in this work is 3 fm, which is smaller than the difference in radii between ^{197}Au and ^{16}O, thus all of the nucleons from ^{16}O will encounter nucleons from ^{197}Au. Different initial configurations of ^{16}O may determine how and when nucleons of a target collide with nucleons from a projectile. This is different from a $^{16}O + ^{16}O$ system [24], in which the random rotation causes target and projectile to brush past each other without collision in some events. We

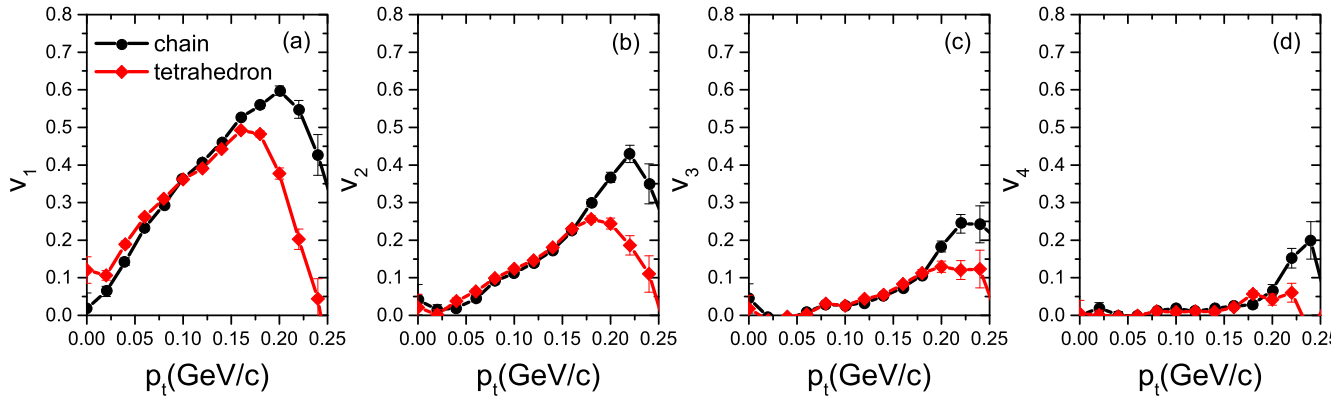

FIG. 5. The same as Fig. 4, but for the transverse momentum p_t dependence of the flow parameters v_1, v_2, v_3, and v_4.

have noted that the difference in final observables caused by the initial configurations is more evident in collisions with larger impact parameter [24].

The collective flow parameters as a function of the transverse momentum p_t are shown in Fig. 5. It can be seen clearly that results calculated with different initial configurations are very close to each other in the low transverse momentum region, but well separated in that of high transverse momentum. The influence of the initial configurations on the flow parameters decreases with increasing order of the flows. The large difference in flows in the high p_t region is a consequence of the fact that nucleons with high p_t usually emit quite early and only undergo a few collisions. After this, those with high p_t nucleons are emitted from the participant zone, and their momenta will be changed only slightly by the weak mean field potential. Then, the influence of different initial configurations can be preserved, so that the difference in flow parameters in the region of high transverse momentum can be visible.

IV. SUMMARY

Within the extended quantum molecular dynamics (EQMD) model, $^{16}\mathrm{O} + {}^{197}\mathrm{Au}$ collisions at beam energy of 40 MeV/nucleon with impact parameter 3 fm were simulated. By considering two different α-clustering configurations (chain and tetrahedron) of ^{16}O in the initialization, the collective flow parameters (v_1, v_2, v_3, and v_4) of free protons were analyzed as a function of both rapidity and the transverse momentum. It was found that the flow parameters are affected by the initial α-clustering configurations, and that this kind of influence decreases with increasing flow order. The difference in flow parameters for the high-transverse-momentum protons can be clearly distinguished because those protons are emitted early and are less influenced by the collision term and mean field potential. In a word, the collective flow of the high-transverse-momentum protons from the mass asymmetric (such as $^{16}\mathrm{O} + {}^{197}\mathrm{Au}$) collisions at 40 MeV/nucleon can be taken as a probe sensitive enough to study the clustering configurations in light nuclei.

ACKNOWLEDGMENTS

This work was supported partly by the National Natural Science Foundation of China under Contracts No. 11421505, No. 11890710, No. 11890714, No. 11605270, and No. U1832182; the Key Research Program of Frontier Sciences of the CAS under Grant No. QYZDJ-SSW-SLH002; and the Strategic Priority Research Program of the CAS under Grants No. XDPB09 and No. XDB16, and the China Postdoctoral Science Foundation under Grant No. 2016LH0045, 2017M621573. We thank Dr. Q. Li, Dr. Y. Wang, and Dr. P. Li for helpful discussions and acknowledge support by the computing server C3S2 at Huzhou University.

[1] B. Hong, Nucl. Sci. Tech. **26**, S20505 (2015); B. Hong, J. K. Ahn, G. Bak *et al.*, *ibid.* **29**, 171 (2018).
[2] B. Wu, J. C. Yang, J. W. Xia *et al.*, Nucl. Instrum. Methods Phys. Res. A **881**, 27 (2018); C. Li, P. Wen, J. Li, G. Zhang, Bing Li, and F. S. Zhang, Nucl. Sci. Tech. **28**, 110 (2017); G.-F. Qu, W.-P. Chai, J.-W. Xia, J. C. Yang, H. Du, Z. S. Li, W. W. Ge, W. H. Zheng, and P. Shang, *ibid.* **28**, 114 (2017); P. Liu, J.-H. Chen, Y.-G. Ma, and S. Zhang, *ibid.* **28**, 55 (2017).
[3] W. von Oertzen, M. Freer, and Y. Kanada-Enyo, Phys. Rep. **432**, 43 (2006).
[4] M. Freer, Rep. Prog. Phys. **70**, 2149 (2007).
[5] J. A. Wheeler, Phys. Rev. **52**, 1083 (1937).
[6] K. Ikeda, N. Takigawa, and H. Horiuchi, Prog. Theor. Phys. Suppl. **6**, 464 (1968).
[7] D. M. Dennison, Phys. Rev. **96**, 378 (1954).
[8] D. Robson, Phys. Rev. Lett. **42**, 876 (1979).
[9] W. Bauhoff, H. Schultheis, and R. Schultheis, Phys. Rev. C **29**, 1046 (1984).
[10] A. Tohsaki, H. Horiuchi, P. Schuck, and G. Ropke, Phys. Rev. Lett. **87**, 192501 (2001).
[11] R. Bijker, in *Symmetries in Nature: Symposium in Memoriam Marcos Moshinsky*, edited by K. B. Wolf, L. Benet, J. M. Torres, and P. O. Hess, AIP Conf. Proc. No. 1323 (AIP, New York, 2010) p. 28.
[12] J.-P. Ebran, E. Khan, T. Niksic, and D. Vretenar, Nature (London) **487**, 341 (2012).
[13] B. Zhou, Y. Funaki, H. Horiuchi, Z. Ren, G. Ropke, P. Schuck, A. Tohsaki, C. Xu, and T. Yamada, Phys. Rev. Lett. **110**, 262501 (2013).
[14] Z. H. Yang, Y. L. Ye, Z. H. Li *et al.*, Phys. Rev. Lett. **112**, 162501 (2014).
[15] S. Elhatisari, E. Epelbaum, H. Krebs, T. A. Lahde, D. Lee, N. Li, B. N. Lu, Ulf-G. Meißner, and G. Rupak, Phys. Rev. Lett. **119**, 222505 (2017).
[16] B. Borderie, Ad. R. Raduta, G. Ademard *et al.*, Phys. Lett. B **755**, 475 (2016).
[17] W. B. He, Y. G. Ma, X. G. Cao, X. Z. Cai, and G. Q. Zhang, Phys. Rev. Lett. **113**, 032506 (2014).
[18] Y. Liu and Y.-L. Ye, Nucl. Sci. Tech. **29**, 184 (2018).
[19] C. Beck, J. Phys.: Conf. Ser. **863**, 012002 (2017)
[20] T. Maruyama, K. Niita, and A. Iwamoto, Phys. Rev. C **53**, 297 (1996).
[21] W. B. He, Y. G. Ma, X. G. Cao, X. Z. Cai, and G. Q. Zhang, Phys. Rev. C **94**, 014301 (2016).
[22] B. S. Huang, Y. G. Ma, and W. B. He, Eur. Phys. J. A **53**, 119 (2017).
[23] B. S. Huang, Y. G. Ma, and W. B. He, Phys. Rev. C **95**, 034606 (2017).
[24] C. C. Guo, W. B. He, and Y. G. Ma, Chin. Phys. Lett. **34**, 092101 (2017).
[25] S. Zhang, Y. G. Ma, J. H. Chen, W. B. He, and C. Zhong, Phys. Rev. C **95**, 064904 (2017).
[26] S. Zhang, Y. G. Ma, J. H. Chen, W. B. He, and C. Zhong, Eur. Phys. J. A **54**, 161 (2018).
[27] Z.-W. Xu, S. Zhang, Y.-G. Ma, J.-H. Chen, and C. Zhong, Nucl. Sci. Tech. **29**, 186 (2018).
[28] J. Aichelin and H. Stoecker, Phys. Lett. B **176**, 14 (1986).
[29] J. Aichelin, Phys. Rep. **202**, 233 (1991).

[30] Y. X. Zhang, Z. X. Li, K. Zhao, H. Liu, and M. B. Tsang, Nucl. Sci. Tech. **24**, 050503 (2013); N. Wang, L. Ou, Y. X. Zhang, and Z. X. Li, Phys. Rev. C **89**, 064601 (2014).
[31] Z.-Q. Feng, Nucl. Sci. Tech. **29**, 40 (2018).
[32] W. B. He, X. G. Cao, Y. G. Ma, D. Q. Fang, H. W. Wang, and G. Q. Zhang, Nucl. Tech. (in Chinese) **37**, 100511 (2014).
[33] S. S. Wang, X. G. Cao, T. L. Zhang, H. W. Wang, G. Q. Zhang, D. Q. Fang, C. Zhong, C. W. Ma, W. B. He, and Y. G. Ma, Nucl. Phys. Rev. **32**, 24 (2015).
[34] D. J. Fields, W. G. Lynch, C. B. Chitwood, C. K. Gelbke, M. B. Tsang, H. Utsunomiya, and J. Aichelin, Phys. Rev. C **30**, 1912 (1984).
[35] J. L. Wile, D. E. Fields, and K. Kwiatkowski, Phys. Rev. C **45**, 2300 (1992).
[36] Y. D. Kim, R. T. de Souza, D. R. Bowman, N. Carlin, C. K. Gelbke, W. G. Gong, W. G. Lynch, L. Phair, M. B. Tsang, and F. Zhu, Phys. Rev. C **45**, 338 (1992).
[37] R. Donangelo and S. R. Souza, Phys. Rev. C **52**, 326 (1995).
[38] R. Donangelo, H. Schulz, K. Sneppen, and S. R. Souza, Phys. Rev. C **50**, R563 (1994).
[39] Y. Wang, C. Guo, Q. Li, H. Zhang, Z. Li, and W. Trautmann, Phys. Rev. C **89**, 034606 (2014).
[40] G. Peilert, H. Stocker, and W. Greiner, Rep. Prog. Phys. **57**, 533 (1994).
[41] Z.-F. Zhang, D.-Q. Fang, and Y.-G. Ma, Nucl. Sci. Tech. **29**, 78 (2018).